Nanoscale

PAPER

Check for updates

Enhancing the interfacial thermal conductance of Si/PVDF by strengthening atomic couplings†

Zhicheng Zong,[a] Shichen Deng,[a] Yangjun Qin,[a] Xiao Wan,[a] Jiahong Zhan,[a] Dengke Ma [b] and Nuo Yang *[a]

Thermal transport across inorganic/organic interfaces attracts interest from both academia and industry due to their wide applications in flexible electronics, *etc*. Here, the interfacial thermal conductance of inorganic/organic interfaces consisting of silicon and polyvinylidene fluoride is systematically investigated using molecular dynamics simulations. Interestingly, it is demonstrated that a modified silicon surface with hydroxyl groups can drastically enhance the conductance by 698%. These results are elucidated based on interfacial couplings and lattice dynamics insights. This study not only provides feasible strategies to effectively modulate the interfacial thermal conductance of inorganic/organic interfaces but also deepens the understanding of the fundamental physics underlying phonon transport across interfaces.

1. Introduction

Inorganic/organic interfaces widely exist in flexible electronics, optoelectronics, photovoltaics, thermoelectrics, *etc*.[1–4] Devices built from hybrid inorganic and organic materials can be designed to combine the complementary strengths of distinct materials.[5,6] PVDF is often referred to as a favorite polymer from the family of organic materials due to its excellent piezoelectric properties, thermal stability, and mechanical strength.[7] In the application of PVDF to wearable flexible devices and batteries, the silicon/polyvinylidene fluoride (Si/PVDF) interface is a commonly utilized and representative interface.[8–10] Recent studies have found that ferroelectric polymers, such as PVDF and nylon, have great potential in thermal modulation.[11,12]

The study of interfacial thermal conductance (ITC) is urgent because the high density of interfaces blocks heat dissipation and causes thermal damage to devices.[13–16] Especially in nanodevices and structures containing high-density interfacial structures, the characteristic size has been reduced to the magnitude of the average free path of energy carriers, and the thermal resistance of atomic-scale interfacial structures cannot be ignored.[17–19] Hence, it is imperative to gain a com-

prehensive understanding of the atomic-scale interfacial thermal transport mechanism and enhance the interfacial thermal conductance accordingly.[20–24]

The modification of surface structures is an effective approach to enhance ITC.[24] Currently, there are various approaches available to enhance ITC, including the utilization of interface defects,[25–27] interlayers[28–31] and surface chemical treatment.[32–38] While the utilization of interface defects does not require the introduction of external materials, more controllable and accurate methods for defect introduction still need to be explored.[39] The introduction of interlayers offers a simpler approach. However, for real materials, the introduction of interlayers alters both the vibrational mismatch and interfacial bonding, leading to a challenging trade-off when selecting the appropriate interlayer.[40] Additionally, these methods cannot significantly enhance interfacial atomic couplings, which limits the improvement of interfacial thermal conductance. Surface chemical treatment has been demonstrated through different experiments as a viable method for modifying surface properties.[38,41–43] This chemical treatment exhibits significant potential in improving the atomic-scale forces and consequently enhancing the ITC of organic/inorganic interfaces.[44] Therefore, in the case of Si/PVDF interfaces, modifying the silicon surface with hydroxyl (OH) groups[45,46] has the potential to enhance ITC.

Molecular dynamics (MD) simulation is a classical approach to simulate thermal transport, where the tracks of atoms are obtained *via* Newton's equation of motion and the empirical potential.[13] Non-equilibrium molecular dynamics (NEMD) can simulate cells with interfacial structures close to reality, providing valuable insight into the physics of ITC.[14,17] By employing NEMD, the heat source/sink is applied to the

[a] School of Energy and Power Engineering, Huazhong University of Science and Technology, Wuhan 430074, China. E-mail: nuo@hust.edu.cn
[b] Phonon Engineering Research Center of Jiangsu Province, Center for Quantum Transport and Thermal Energy Science, Institute of Physics and Interdisciplinary Science, School of Physics and Technology, Nanjing Normal University, Nanjing 210023, China
† Electronic supplementary information (ESI) available. See DOI: https://doi.org/10.1039/d3nr03706a

left/right end of Si/PVDF structures, which records temperature difference and heat flux at the interface. Besides, more valuable information about atomic vibrations and the forces between atoms can also be recorded.

In this work, the interfacial thermal conductance (ITC) of Si/PVDF is enhanced by modifying the surface with OH groups. The study was performed using non-equilibrium molecular dynamics (NEMD) simulations. First, Si/PVDF interfaces with intrinsic and modified Si with OH groups were constructed. Second, the effects of intrinsic and modified Si on ITC were studied. Third, an analysis of atomic couplings and lattice dynamics was carried out to explain the difference between the ITC of intrinsic and modified Si surfaces. Lastly, the effect of temperature difference of the Si/PVDF interface on ITC was studied and the outlook of future research is proposed.

2. Structure and methods

The simulation cells of different Si/PVDF were formed and are shown in Fig. 1(a)–(f). In order to investigate the roles of OH groups in interfacial heat transfer, the intrinsic silicon (In-Si) and modified silicon (Mod-Si) surfaces facing PVDF were structured. Furthermore, poled-PVDF (P-PVDF), unpoled-PVDF (U-PVDF), and amorphous PVDF (A-PVDF) were structured to explore the effects of modulation on ITC. All the details of the structures are provided in ESI 1.†

MD simulations were implemented using the Large-scale Atomic/Molecular Massively Parallel Simulator (LAMMPS)[47] with the force field of PCFF/Lennard-Jones/Tersoff.[48,49] The PCFF force field, designed for modeling polymers, has demonstrated successful applications in simulating the thermal transport properties of PVDF, and showed excellent agreement with experimental results.[11,48] The Tersoff potential is employed for Si, which is widely used to study thermal properties.[49,50] Additionally, the Lennard-Jones (LJ) potential is commonly utilized in ITC simulations.[51,52] The parameters of LJ can properly describe the interactions between different materials.[47]

Prior to the recording of heat flux, the structures underwent a full relaxation process. Following the relaxation process through MD simulation, the initial structures (Fig. 1) evolved into stable and optimized structures (Fig. S1†), accompanied by appropriate simulation cell sizes. The combination of time and ensemble sampling was employed to obtain the average. Four independent simulations were conducted with different initial conditions. More details of simulations are provided in ESI 2 through 5.†

3. Results and discussion

The relaxed structures and temperature profiles are shown in Fig. 2. First, the interfacial temperature difference and the heat flux were recorded (details in ESI 3 and 4†). Then, the ITC and the total thermal conductance (TTC) were calculated. The TTC includes the conductance of Si, the conductance of PVDF, and ITC. For Mod-Si/PVDF interfaces, the intermediate layer OH groups are taken into account in the interface thermal resistance, where the interfacial temperature difference is $\Delta T_{\text{Si/OH/PVDF}}$.

The ITC values of different Si/PVDF interfaces are shown in Fig. 3(a). By employing NEMD simulation, the ITC values of the six different simulation cells above are determined at 300 K. Among the same silicon surfaces, it is observed that A-PVDF exhibits a higher ITC than U-PVDF, whereas U-PVDF demonstrates a higher ITC than P-PVDF. Previous studies[53–55]
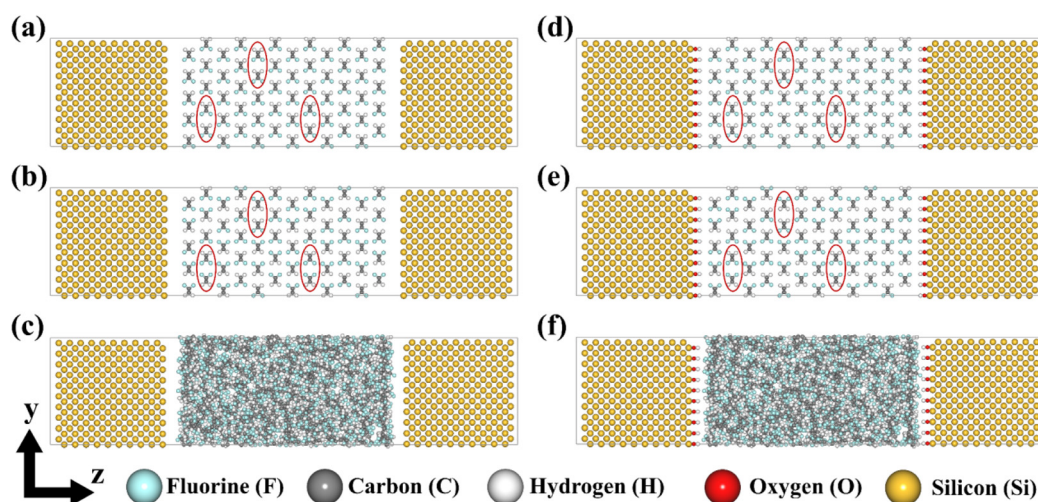

Fig. 1 Schematics of the interface structures are shown in the yz plane: (a) In-Si/P-PVDF interface, (b) In-Si/U-PVDF interface, (c) In-Si/A-PVDF interface, (d) Mod-Si/P-PVDF interface, (e) Mod-Si/U-PVDF interface and (f) Mod-Si/A-PVDF interface. The chain length of PVDF in the structure is 10 units, and the along-chain (x) direction in the structure is periodic.
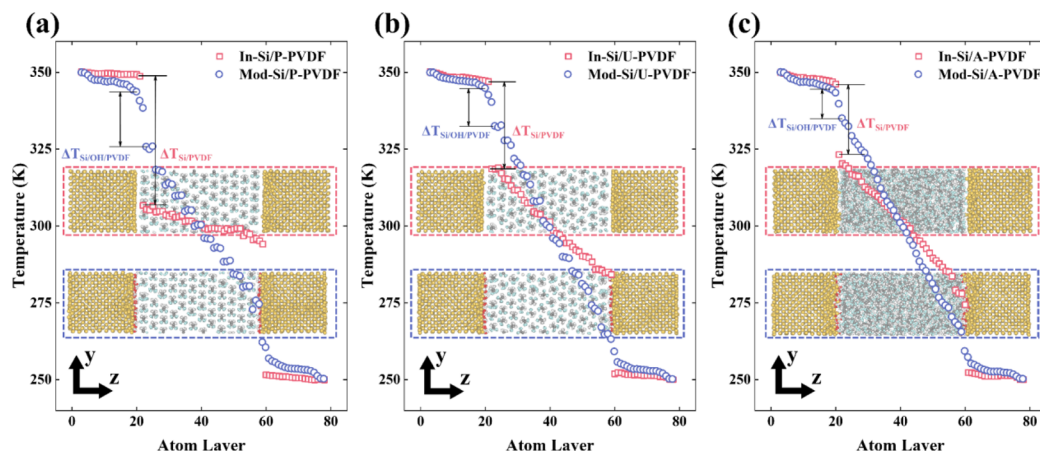
Fig. 2 The relaxed structures and the temperature profiles of (a) In-Si/P-PVDF and Mod-Si/P-PVDF, (b) In-Si/U-PVDF and Mod-Si/U-PVDF, and (c) In-Si/A-PVDF and Mod-Si/A-PVDF.
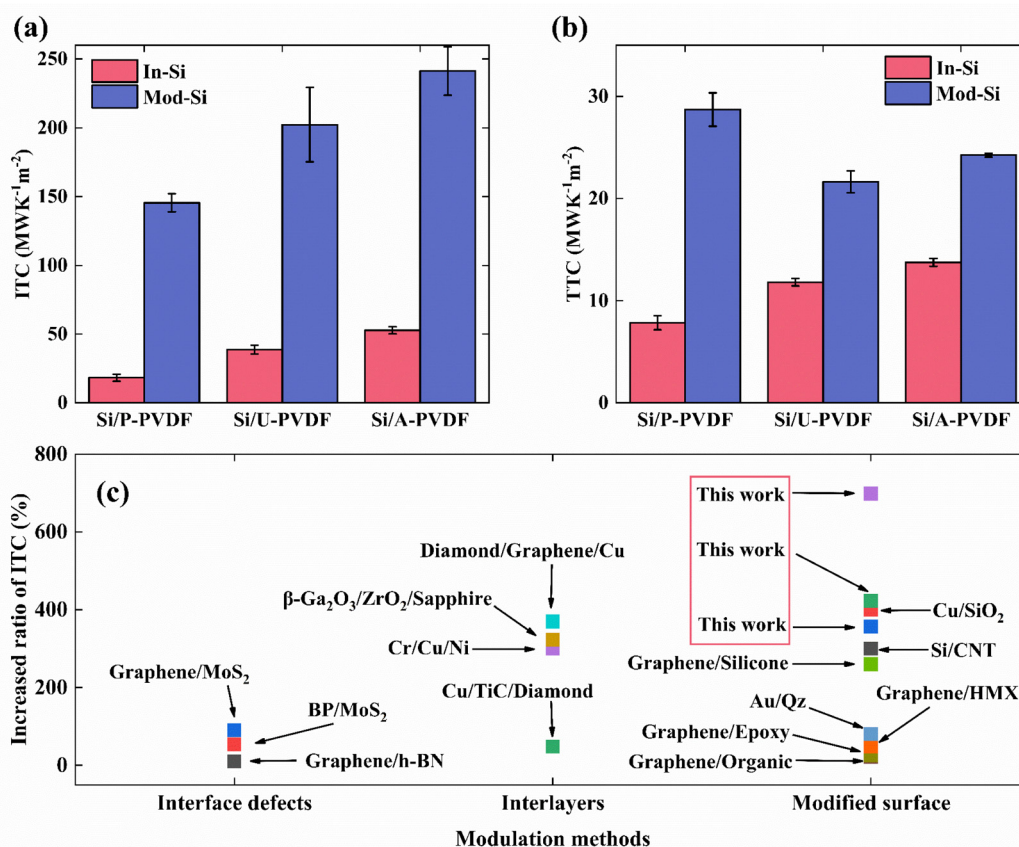

Fig. 3 (a) ITC of the PVDF/Si interface: for Si/P-PVDF, Si/U-PVDF, and Si/A-PVDF interfaces, through modification of the Si surface ITC can be increased by 698%, 423%, and 357%. (b) TTC of composite structures: for Si/P-PVDF, Si/U-PVDF, and Si/A-PVDF composite structures, through modification of the Si surface TTC of composite structures can be increased by 266%, 83%, and 76%. (c) Increased ratio of ITC *versus* those of other modulation methods (graphene/h-BN,[25] BP/MoS₂,[26] graphene/MoS₂,[27] Cu/TiC/diamond,[28] Cr/Cu/Ni,[29] β-Ga₂O₃/ZrO₂/sapphire,[30] diamond/graphene/copper,[31] graphene/organic,[32] graphene/epoxy,[33] graphene/HMX,[34] Au/Qz,[35] graphene/silicone,[36] Si/CNT[37] and Cu/SiO₂ [38]).

have also consistently indicated that amorphous/crystalline interfacial structures exhibit better ITC performance than crystalline/crystalline ones.

In terms of the interface, the match/mismatch of two materials significantly influences its ITC.[13,17] When one side is an amorphous structure, the range of phonon modes is much

broader than that in a crystal. This may lead to an abundance of matching phonon modes across the interface, which facilitates efficient interfacial thermal conduction.[56] Furthermore, the elastic interaction and diffusive scattering at amorphous/crystalline interfaces can independently generate a number of thermal channels for energy transmissions, compared to crystalline/crystalline interfaces.[54,57] These phenomena contribute to good thermal coupling, consequently enhancing ITC. The observed difference in ITC can primarily be attributed to the higher level of disorder in A-PVDF, which results in stronger coupling and match with the interface. On the other hand, P-PVDF is characterized as the weakest among the PVDF, contributing to its lowest ITC.

The ITC of the modified Si surface is much larger, up to 698%, than that of the intrinsic case. It is observed that the modifications applied to the Si surface using the properties of the OH groups led to a substantial enhancement in the ITC. Compared with the In-Si/PVDF interface, the ITC values of Mod-Si/P-PVDF, Mod-Si/U-PVDF, and Mod-Si/A-PVDF interfaces are increased by 698%, 423%, and 357%, respectively. More importantly, for Mod-Si/P-PVDF interfaces, the ITC experienced a substantial increase from 18 ± 3 to 145 ± 7 MW K^{-1} m^{-2} (698%) compared to that of the In-Si/P-PVDF interface. As plotted in Fig. 3(c), the enhancement of this work is compared with the results of other methods, such as those using interface defects[25–27] and interlayers.[28–31] The results in this work demonstrate remarkable potential for significantly enhancing ITC compared to those of other existing methods or studies.

Besides, the thermal conductance of the whole composite structure is studied, as shown in Fig. 3(b). Through modification of the Si surface, the TTC values of Si/P-PVDF, Si/U-PVDF, and Si/A-PVDF can be increased by 266%, 83%, and 76%, respectively. Notably, the thermal conductivity of Si and PVDF remained unchanged before and after the modification of the Si surface (details in ESI 5†). The primary determinant of thermal conductance variation in the composite system is attributed to alterations in ITC. On the one hand, the result indicates that by modifying the Si surface with hydroxy groups, the thermal transport of both the Si/PVDF interface and total composite structures can be largely increased. On the other hand, the results also show that thermal transport across the interface plays a significant role at the nanoscale.

To elucidate the mechanism behind ITC changes, the interfacial atomic structures are plotted in Fig. 4(a). The local structure of the interface shows the modified Si surface and the atoms in the PVDF at the interface. In the case of In-Si, the interaction with PVDF is primarily governed by van der Waals forces. Conversely, in the case of Mod-Si, the interaction involves both van der Waals and coulombic forces with PVDF, thereby strengthening the atomic couplings. It has been observed in the relaxed structure (Fig. 2) that the proximity of the F atoms to the OH groups is evident. This reveals that the
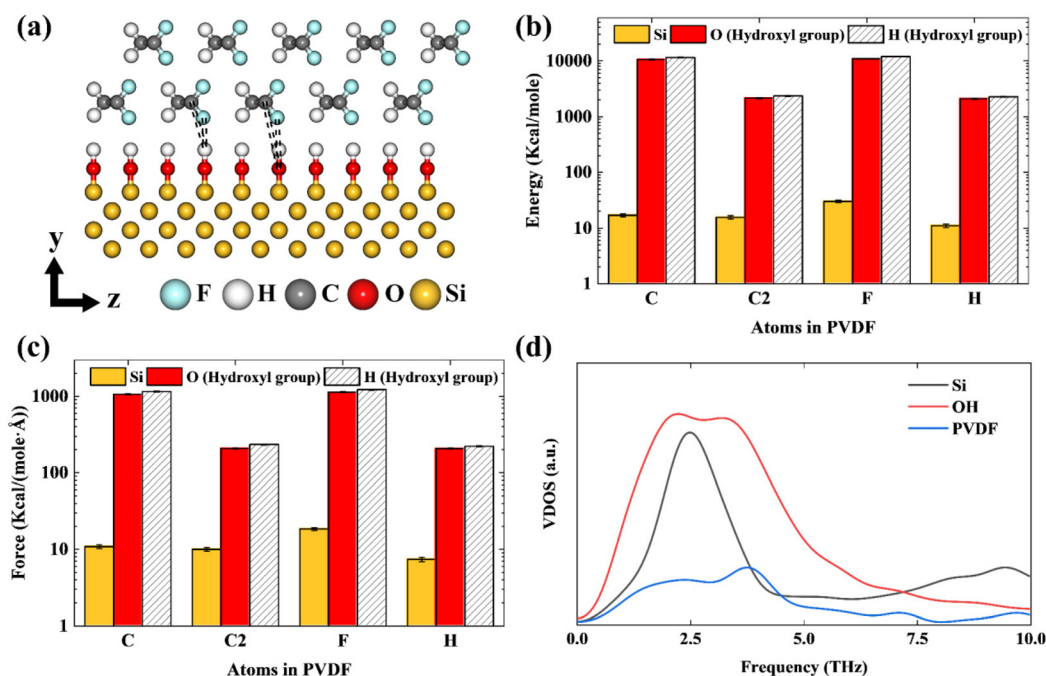

Fig. 4 (a) Schematic of atomic force in Mod-Si/P-PVDF composite structures. After the modification of the Si surface, the main atomic couplings at the interface undergo transformation from van der Waals forces to coulombic forces. (b) Total energy and (c) force of interaction between different groups of atoms. The OH groups on the modified Si surface exhibit a stronger interaction with the atoms in PVDF, leading to a substantial enhancement in ITC. (d) The vibrational density of states (VDOS) below 10.0 THz of Mod-Si/P-PVDF composite structures indicates that the coincidence area of PVDF and Si (16.1%) is slightly smaller than that of PVDF and OH (16.4%).

OH groups govern the interaction between Mod-Si and PVDF, as shown in Fig. 4(a).

Generally, stronger atomic coupling can cause more efficient heat conduction. This is primarily because stronger interfacial couplings provide multiple paths for thermal transport, which can exert a significant influence on the transmission probabilities across interfaces.[14] Then total energy and force of interaction between different groups of atoms are quantitatively compared in Fig. 4(b) and (c), where C and C2 represent different types of carbon atoms in PVDF (details in

ESI 2†). When averaging and calculating the values of energy and force of atomic interaction, all atoms are considered and counted (details in ESI 6†). The observations indicate that the OH groups on the modified silicon surface exhibit a stronger interaction with the atoms in PVDF, which brings organic molecules closer to the interface, thereby further increasing the interface binding energy and the transmission probabilities across the interface.[14,42] As a result, strong atomic coupling contributes significantly to the enhanced ITC.

To further understand the mechanism, the vibrational density of states (VDOS) is calculated and analyzed qualitatively (details in ESI 7†). For VDOS below 10.0 THz of Mod-Si/P-PVDF composite structures, the coincidence area of PVDF and Si (16.1%) is marginally smaller than that of PVDF and OH (16.4%), as shown in Fig. 4(d). Based on the theoretical model,[13,58] the OH groups situated on the surface of modified silicon display a higher degree of matching with PVDF, resulting in an increased supply of thermal transport channels and thus enhanced ITC. However, the impact of VDOS recombination on the enhancement of ITC is relatively limited. In contrast, the main driving force behind the increase is the elevation of strong atomic coupling.

Furthermore, the temperature dependence of ITC is studied from 300 K to 500 K (Fig. 5). The results demonstrate a positive correlation between ITC and temperature, indicating that an increase in temperature leads to a corresponding increase in ITC, particularly for the Mod-Si/U-PVDF interface. The increase in temperature promotes the occurrence of multi-phonon processes at the interface, thus creating new pathways for heat transport.[27,59] The In-Si/U-PVDF interface exhibits a weak interaction that hinders the transportation of high-frequency phonons. Conversely, the Mod-Si/U-PVDF interface demonstrates a strong interaction, which facilitates the transportation of high-frequency phonons. Besides, the inelastic high order
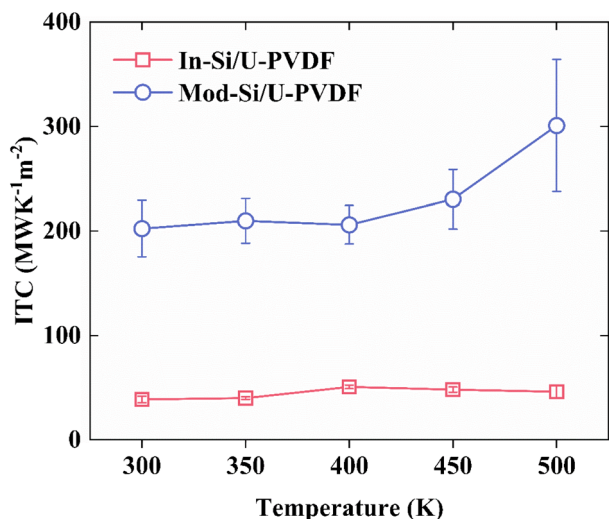
Fig. 5 ITC of In-Si/U-PVDF and Mod-Si/U-PVDF interfaces varies with different temperatures. High-frequency modes stimulated at high temperatures can be transmitted across the interface through evanescent modes, facilitated by the inelastic three-phonon scattering process, resulting in the enhancement of ITC.
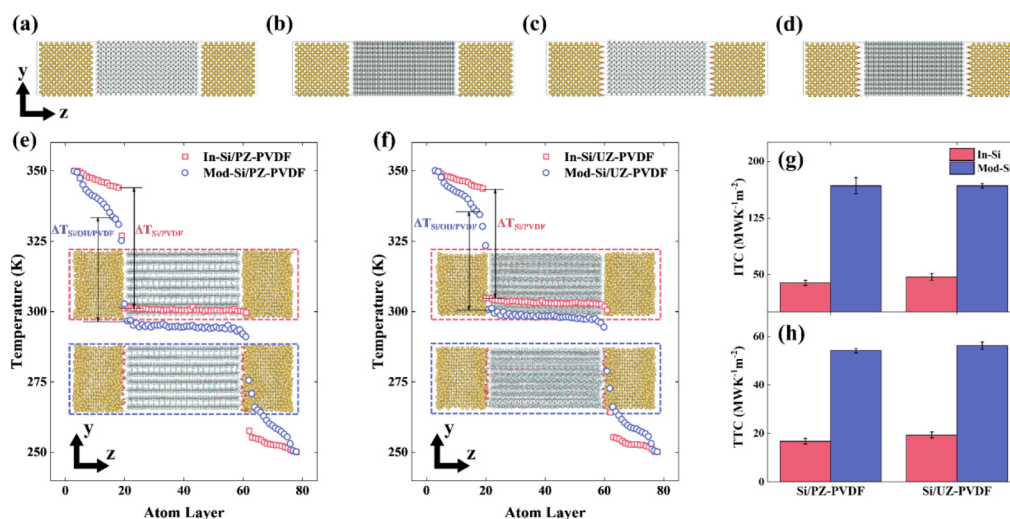

Fig. 6 Schematics of the interface structures. (a) In-Si/PZ-PVDF interface, (b) In-Si/UZ-PVDF interface, (c) Mod-Si/PZ-PVDF interface, and (d) Mod-Si/UZ-PVDF interface. The chain length of PVDF is 20 units (5.4 nm). The relaxed structures and the temperature profiles of (e) In-Si/PZ-PVDF and Mod-Si/PZ-PVDF, and (f) In-Si/UZ-PVDF and Mod-Si/UZ-PVDF. The corresponding (g) ITC values and (h) TTC values.

phonon scattering process also results in the enhancement of ITC.[13] The introduction of OH groups on the Si surface introduces numerous phonon modes at higher frequencies (as shown in Fig. S7†), which contribute to the increased ITC variations at the interface with the increase of temperature.

It is noted that the system does not melt at 500 K which surpasses the melting point of amorphous PVDF (450 K).[11] The melting points of polymers increase with chain length and lamellar crystal thickness.[60–62] In simulations shown in Fig. 5, the studied structures of PVDF are crystalline-like, and periodic boundary conditions are applied, simulating an infinite chain length and lamellar crystal thickness. Therefore, the melting point in systems is higher than 450 K, and the system does not melt at 500 K. These findings are consistent with similar phenomena reported in previous studies conducted using MD simulations, such as PE,[63] PEO,[64] PEDOT,[65] PVDF[11] and nylon.[12]

The strategy to enhance the ITC and TTC of Si/PVDF composites is also applicable to other PVDF structures. In the above text, the heat flow perpendicular to the chain direction, an orientation where PVDF has lower thermal conductivity, is focused on. Then, the thermal transport along the orientation direction for the structures with/without the modified Si surface was investigated (details in ESI 8†).

Fig. 6(a)–(d) show the interfacial structures of the poled PVDF chain oriented in the z-direction (PZ-PVDF) and the unpoled-PVDF chain oriented in the z-direction (UZ-PVDF). The relaxed structures and the temperature profiles are shown in Fig. 6(e) and (f). Fig. 6(g) and (h) show the ITC values and TTC values of different structures. For Si/PZ-PVDF and Si/UZ-PVDF, the modification of the Si surface results in ITC increases of 331% and 256%, respectively. Besides, there are TTC enhancements of 224% and 191% for the composite structures, respectively.

4.   Conclusion

In summary, the modification effect on the thermal transport across the Si/PVDF interface is investigated using molecular dynamics simulations. The Si/PVDF interfaces are modified with hydroxyl groups, where atomic couplings between Si and PVDF are strengthened. The interfacial thermal conductance across modified interfaces is significantly enhanced compared with that of the intrinsic interface. The ITC value across Mod-Si/P-PVDF increased from 18 ± 3 to 145 ± 7 MW K^{-1} m^{-2} (698%). The interfacial coupling analysis reveals that the increased interfacial bonding leads to a dramatic increase in ITC. Then, the VDOS results show that the modification of the Si surface leads to more phonon transport across the interface. Moreover, the ITC values of Mod-Si/U-PVDF and In-Si/U-PVDF simulated at different temperatures are calculated, and the results show that ITC could be enhanced with the increment of temperature. It is believed that fine-tuning the process of surface modification can achieve an optimal structure of in-

organic/organic interfaces with both higher interfacial adhesion and better mechanical properties. This study illustrates an effective avenue to tune thermal transport performance across inorganic/organic interfaces for thermal management and energy efficiency applications. However, in certain devices with high mechanical requirements, the application may be limited. This drawback can be mitigated by exploring appropriate silicon surface modification methods suitable to specific devices.

Conflicts of interest

The authors have no conflicts to declare.

Acknowledgements

References

1 X. Tang, H. Shen, S. Zhao, N. Li and J. Liu, *Nat. Electron.*, 2023, **6**, 109–118.
2 M. U. Rothmann, J. S. Kim, J. Borchert, K. B. Lohmann, C. M. O'Leary, A. A. Sheader, L. Clark, H. J. Snaith, M. B. Johnston, P. D. Nellist and L. M. Herz, *Science*, 2020, **370**, eabb5940.
3 K. Kim, E. Vetter, L. Yan, C. Yang, Z. Wang, R. Sun, Y. Yang, A. H. Comstock, X. Li, J. Zhou, L. Zhang, W. You, D. Sun and J. Liu, *Nat. Mater.*, 2023, **22**, 322–328.
4 J. C. Blancon, J. Even, C. C. Stoumpos, M. G. Kanatzidis and A. D. Mohite, *Nat. Nanotechnol.*, 2020, **15**, 969–985.
5 T. Schultz, D. Lungwitz, E. Longhi, S. Barlow, S. R. Marder and N. Koch, *Adv. Funct. Mater.*, 2020, **31**, 2010174.
6 J. A. Malen, S. K. Yee, A. Majumdar and R. A. Segalman, *Chem. Phys. Lett.*, 2010, **491**, 109–122.
7 Z.-X. Wang and W.-Q. Liao, *Science*, 2022, **375**, 1353–1354.
8 D. Y. Lee, H. Kim, H. M. Li, A. R. Jang, Y. D. Lim, S. N. Cha, Y. J. Park, D. J. Kang and W. J. Yoo, *Nanotechnology*, 2013, **24**, 175402.
9 Y. Lai, H. Li, Q. Yang, H. Li, Y. Liu, Y. Song, Y. Zhong, B. Zhong, Z. Wu and X. Guo, *Ind. Eng. Chem. Res.*, 2022, **61**, 6246–6268.
10 S. Chen, X. Li, K. Yao, F. E. H. Tay, A. Kumar and K. Zeng, *Polymer*, 2012, **53**, 1404–1408.
11 S. Deng, J. Yuan, Y. Lin, X. Yu, D. Ma, Y. Huang, R. Ji, G. Zhang and N. Yang, *Nano Energy*, 2021, **82**, 105749.
12 S. Deng, D. Ma, G. Zhang and N. Yang, *J. Mater. Chem. A*, 2021, **9**, 24472–24479.
13 J. Chen, X. Xu, J. Zhou and B. Li, *Rev. Mod. Phys.*, 2022, **94**, 025002.

14 C. Monachon, L. Weber and C. Dames, *Annu. Rev. Mater. Res.*, 2016, **46**, 433–463.

15 D. G. Cahill, P. V. Braun, G. Chen, D. R. Clarke, S. Fan, K. E. Goodson, P. Keblinski, W. P. King, G. D. Mahan, A. Majumdar, H. J. Maris, S. R. Phillpot, E. Pop and L. Shi, *Appl. Phys. Rev.*, 2014, **1**, 011305.

16 R. Qi, R. Shi, Y. Li, Y. Sun, M. Wu, N. Li, J. Du, K. Liu, C. Chen, J. Chen, F. Wang, D. Yu, E.-G. Wang and P. Gao, *Nature*, 2021, **599**, 399–403.

17 A. Giri and P. E. Hopkins, *Adv. Funct. Mater.*, 2020, **30**, 1903857.

18 L. Yang, X. Wan, D. Ma, Y. Jiang and N. Yang, *Phys. Rev. B*, 2021, **103**, 155305.

19 T. Jiang, X. Zhang, S. Vishwanath, X. Mu, V. Kanzyuba, D. A. Sokolov, S. Ptasinska, D. B. Go, H. G. Xing and T. Luo, *Nanoscale*, 2016, **8**, 10993–11001.

20 L. Yang, B. Latour and A. J. Minnich, *Phys. Rev. B*, 2018, **97**, 205306.

21 Y. Tao, C. Wu, H. Qi, C. Liu, X. Wu, M. Hao, Z. Wei, J. Yang and Y. Chen, *Nanoscale*, 2020, **12**, 14838–14846.

22 J. Wang, Z. Wang, K. Yang, N. Chen, J. Ni, J. Song, Q. Li, F. Sun, Y. Liu and T. Fan, *Adv. Funct. Mater.*, 2022, **32**, 2206545.

23 B. Wu, Y. Li, W. Chen, B. Ding, P. Chen, R. Xia and J. Qian, *J. Mater. Chem. A*, 2022, **10**, 13858–13867.

24 S. Park, J. Jang, H. Kim, D. I. Park, K. Kim and H. J. Yoon, *J. Mater. Chem. A*, 2020, **8**, 19746–19767.

25 X. Liu, G. Zhang and Y. W. Zhang, *Nano Lett.*, 2016, **16**, 4954–4959.

26 B. Wu, M. Zhou, D. Xu, J. Liu, R. Tang and P. Zhang, *Surf. Interfaces*, 2022, **32**, 102119.

27 Y. Liu, W. Wu, S. Yang and P. Yang, *Surf. Interfaces*, 2022, **28**, 101640.

28 G. Chang, F. Sun, L. Wang, Z. Che, X. Wang, J. Wang, M. J. Kim and H. Zhang, *ACS Appl. Mater. Interfaces*, 2019, **11**, 26507–26517.

29 D. Ma and L. Zhang, *J. Phys.: Condens. Matter*, 2020, **32**, 425001.

30 J. Noh, P. R. Chowdhury, M. Segovia, S. Alajlouni, M. Si, A. R. Charnas, S. Huang, K. Maize, A. Shakouri, X. Xu, X. Ruan and P. D. Ye, *IEEE Trans. Electron Devices*, 2022, **69**, 1186–1190.

31 H. Cao, Z. Tan, M.-H. Lu, M. Ji, X.-J. Yan, C. Di, M. Yuan, Q. Guo, Y. Su, A. Addad, Z. Li and D.-B. Xiong, *Carbon*, 2019, **150**, 60–68.

32 S. Lin and M. J. Buehler, *Nanotechnology*, 2013, **24**, 165702.

33 T.-Y. Wang and J.-L. Tsai, *Comput. Mater. Sci.*, 2016, **122**, 272–280.

34 Z. Cao, X. Huang, Y. Wang, C. Zhang, X. Xue, G. He, H. Wang and Y. Ni, *J. Mater. Sci.*, 2023, **58**, 4668–4678.

35 M. D. Losego, M. E. Grady, N. R. Sottos, D. G. Cahill and P. V. Braun, *Nat. Mater.*, 2012, **11**, 502–506.

36 S.-Y. Lee, P. Singh and R. L. Mahajan, *Carbon*, 2019, **145**, 131–139.

37 H.-B. Fan, K. Zhang and M. M. F. Yuen, *J. Appl. Phys.*, 2009, **106**, 034307.

38 P. J. O'Brien, S. Shenogin, J. Liu, P. K. Chow, D. Laurencin, P. H. Mutin, M. Yamaguchi, P. Keblinski and G. Ramanath, *Nat. Mater.*, 2013, **12**, 118–122.

39 Y. Xu, R. Ge, J. Yang, J. Li, S. Li, Y. Li, J. Zhang, J. Feng, B. Liu and W. Li, *J. Energy Chem.*, 2022, **74**, 45–71.

40 D. Ma, Y. Xing and L. Zhang, *J. Phys.: Condens. Matter*, 2023, **35**, 053001.

41 P. Zhang, P. Yuan, X. Jiang, S. Zhai, J. Zeng, Y. Xian, H. Qin and D. Yang, *Small*, 2018, **14**, 1702769.

42 X. D. Zhang, G. Yang and B. Y. Cao, *Adv. Mater. Interfaces*, 2022, **9**, 2200078.

43 F. Sun, T. Zhang, M. M. Jobbins, Z. Guo, X. Zhang, Z. Zheng, D. Tang, S. Ptasinska and T. Luo, *Adv. Mater.*, 2014, **26**, 6093–6099.

44 F. Zou and A. Manthiram, *Adv. Energy Mater.*, 2020, **10**, 2002508.

45 E. C. Muñoz, C. Díaz, E. Navarrete, R. Henríquez, R. Schrebler, R. Córdova, R. Marotti and C. Heyser, *Arabian J. Chem.*, 2019, **12**, 5125–5133.

46 P. Thissen, T. Peixoto, R. C. Longo, W. Peng, W. G. Schmidt, K. Cho and Y. J. Chabal, *J. Am. Chem. Soc.*, 2012, **134**, 8869–8874.

47 A. P. Thompson, H. M. Aktulga, R. Berger, D. S. Bolintineanu, W. M. Brown, P. S. Crozier, P. J. in 't Veld, A. Kohlmeyer, S. G. Moore, T. D. Nguyen, R. Shan, M. J. Stevens, J. Tranchida, C. Trott and S. J. Plimpton, *Comput. Phys. Commun.*, 2022, **271**, 108171.

48 H. Sun, S. J. Mumby, J. R. Maple and A. T. Hagler, *J. Am. Chem. Soc.*, 1994, **116**, 2978–2987.

49 J. Tersoff, *Phys. Rev. B: Condens. Matter Mater. Phys.*, 1988, **38**, 9902–9905.

50 Y. Lee, S. Lee and G. S. Hwang, *Phys. Rev. B: Condens. Matter Mater. Phys.*, 2011, **83**, 125202.

51 Y. Hong, J. Zhang and X. C. Zeng, *Nanoscale*, 2016, **8**, 19211–19218.

52 S. Tian, Z. Xu, S. Wu, T. Luo and G. Xiong, *Int. J. Heat Mass Transfer*, 2022, **195**, 123134.

53 A. Giri, P. E. Hopkins, J. G. Wessel and J. C. Duda, *J. Appl. Phys.*, 2015, **118**, 165303.

54 K. Gordiz and A. Henry, *J. Appl. Phys.*, 2017, **121**, 025102.

55 A. Giri, S. W. King, W. A. Lanford, A. B. Mei, D. Merrill, L. Li, R. Oviedo, J. Richards, D. H. Olson, J. L. Braun, J. T. Gaskins, F. Deangelis, A. Henry and P. E. Hopkins, *Adv. Mater.*, 2018, **30**, 1804097.

56 S. W. Fong, A. Sood, L. Chen, N. Kumari, M. Asheghi, K. E. Goodson, G. A. Gibson and H. S. P. Wong, *J. Appl. Phys.*, 2016, **120**, 015103.

57 A. Giri, J. L. Braun and P. E. Hopkins, *J. Appl. Phys.*, 2016, **119**, 235305.

58 Z.-C. Zong, D.-K. Pan, S.-C. Deng, X. Wan, L.-N. Yang, D.-K. Ma and N. Yang, *Acta Phys. Sin.*, 2023, **72**, 034401.

59 K. Ren, Y. Chen, H. Qin, W. Feng and G. Zhang, *Appl. Phys. Lett.*, 2022, **121**, 082203.

60 G. Ungar, J. Stejny, A. Keller, I. Bidd and M. C. Whiting, *Science*, 1985, **229**, 386–389.

61 G. Strobl, *Prog. Polym. Sci.*, 2006, **31**, 398–442.

62 F. P. V. Koch, J. Rivnay, S. Foster, C. Müller, J. M. Downing, E. Buchaca-Domingo, P. Westacott, L. Yu, M. Yuan, M. Baklar, Z. Fei, C. Luscombe, M. A. McLachlan, M. Heeney, G. Rumbles, C. Silva, A. Salleo, J. Nelson, P. Smith and N. Stingelin, *Prog. Polym. Sci.*, 2013, **38**, 1978–1989.

63 T. Zhang and T. Luo, *J. Appl. Phys.*, 2012, **112**, 094304.

64 H. Meng, X. Yu, H. Feng, Z. Xue and N. Yang, *Int. J. Heat Mass Transfer*, 2019, **137**, 1241–1246.

65 X. Yu, R. Li, T. Shiga, L. Feng, M. An, L. Zhang, J. Shiomi and N. Yang, *J. Phys. Chem. C*, 2019, **123**, 26735–26741.

Electronic supplementary information

Enhancing interfacial thermal conductance of Si/PVDF by strengthening atomic couplings

Zhicheng Zong[1], Shichen Deng[1], Yangjun Qin[1], Xiao Wan[1], Jiahong Zhan[1], Dengke Ma[2], Nuo Yang[1*]

1. School of Energy and Power Engineering, Huazhong University of Science and Technology, Wuhan 430074, China.

2. Phonon Engineering Research Center of Jiangsu Province, Center for Quantum Transport and Thermal Energy Science, Institute of Physics and Interdisciplinary Science, School of Physics and Technology, Nanjing Normal University, Nanjing 210023, China

*Corresponding email: nuo@hust.edu.cn (N.Y)

ESI 1. Structures details

The inorganic/organic material interface formed by PVDF and Si is shown in Fig. 1(a)-(f). The left and right silicon layers are face-centered cubic in the direction of [001] from left to right, and the left and right sides each contain 20 layers of silicon atoms with a cross-sectional area of 2.6 nm × 2.6nm. PVDF is placed in the middle of two silicon substrates. The interface structure is sufficiently large to include most of the important phonon modes contributing to the interfacial thermal transport and thus can exclude the size effect[1].

The intrinsic silicon (In-Si) is structured, as shown in Fig. 1(a)-(c). To study the roles of hydroxyl groups in the interfacial heat transfer, the modified silicon (Mod-Si) surfaces facing PVDF are structured, as shown in Fig. 1(d)-(f). PVDF arrays are constructed by aligning 60 straight PVDF chains and placed in the middle of two silicon substrates, as shown in Fig. 1(a), (b), (d), and (e). For poled-PVDF (P-PVDF), as shown in Fig. 1(a) and (d), the orientations of all chains along the y direction are the same, generating a net dipole moment along x of the whole system. While for unpoled-PVDF (U-PVDF), as shown in Fig. 1(b) and (e), half the chains orientate oppositely with the other half along the x-direction (direction of dipole moment), the dipole moments of two parts cancel each other out, resulting in zero dipole moment of the whole system.

Besides, amorphous PVDF (A-PVDF) is also structured and placed in the middle of two silicon substrates, as shown in Fig. 1 (c) and (f). When constructing A-PVDF, a single PVDF chain contains 20 carbon atoms. Then 60 of these single PVDF chains are randomly packed into a supercell. After minimization, a NPT ensemble (a constant number of atoms, pressure and temperature) is used to increase the system temperature from 300 K to 600 K by a constant rate of 50 K/ns, and then a 12 ns NPT run at 600 K is used to generate PVDF melt with a fully relaxed amorphous structure. The system is then quenched to 300 K by a constant rate of 50 K/ns and equilibrated in the NPT ensemble for 1 ns to converge the density.

ESI 2. Molecular dynamics simulation details

The Non-equilibrium molecular dynamics (NEMD) simulation method is used to calculate the thermal transport properties of Si/PVDF interface. And the detailed setting parameters of all NEMD simulations are listed in Table S1. Noting that kB is the Boltzmann constant, V is the system volume, T is the temperature, E is total kinetic energy of the group of atoms, N is the number of total atoms, and the angular bracket denotes an ensemble average. All NEMD simulations in this work are performed by the large-scale atomic/molecular massively parallel simulator (LAMMPS) package[2]. The interactions between atoms are described by the polymer consistent force field (PCFF)[3] which includes anharmonic bonding terms and is intended for applications in polymers and organic materials. Table S2 to S5 list the specific parameters of potential function in NEMD simulation. The long-range Coulombic force is ignored. Periodic boundary conditions are applied in the x and y directions, while nonperiodic boundary conditions are used in the z-direction. And the velocity Verlet algorithm is employed to integrate equations of motion. 0.25 fs and 10 Å are chosen as time step and cutoff distance for the Lennard-Jones interaction, respectively. In addition, 4 independent simulations with different initial conditions are conducted to get a better average. The simulation structures are simulated in NPT ensembles at target temperatures and 1 atm for 1ns to obtain the optimized structures and simulation cell sizes, then followed by NVT (for 1ns) and NVE (for 2ns) ensembles before collecting heat flux of z direction (across interface) in NVE ensembles for 5 ns.

Table S1 Non-Equilibrium molecular dynamics (NEMD) simulation details.

Method	Non-Equilibrium molecular dynamics (NEMD)		
Potential	PCFF/Lennard-Jones/Tersoff	Time step	0.25 fs
Thermostat	Langevin	Heat source	350 K
		Heat sink	250 K
Simulation process			
Ensemble	Setting		Purpose
NPT	Boundary condition	x, y, z: p, p, p	Relax Structure
	Runtime	1 ns	
NVT	Boundary condition	x, y, z: p, p, f	Relax Structure
	Runtime	1 ns	
NVE	Boundary condition	x, y, z: p, p, f	
	Runtime	2 ns	
NVE	Boundary condition	x, y, z: p, p, f	Reach information
	Runtime	5 ns	
Recorded physical quantity			
Temperature	$\langle E \rangle = \sum_i \frac{1}{2} m_i v_i^2 = \frac{3}{2} N k_B T_{MD}$		
Heat flux	$J = \frac{1}{N_t} \sum_{i=1}^{N_t} \frac{\Delta \varepsilon_i}{2 \Delta t}$		
Interfacial thermal conductance	$G = \frac{J}{A \cdot \Delta T}$		

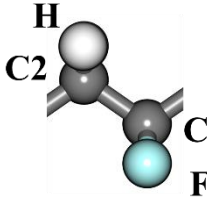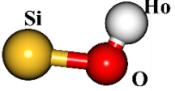Table S2 The types of atoms in PVDF chain and hydroxyl group.

Structures		Atom types	Charge (e)
PVDF chain		C	0.5
		C2	-0.106
		F	-0.25
		H	0.053
Hydroxyl group		O	-0.34
		Ho	0.34

Table S3 The types of potential functions contained in PCFF force field.

Potential function in PVDF and hydroxyl group
Bond: class2
Angle: class2
Dihedral: class2
Improper: class2
Non-bonding potential: lj/class2/coul/cut 10.0
Special bond: lj 0.0 0.0 0.5 coul 0.0 0.0 0.5

Table S4 Bond parameters.

Bond	r_0 (Å)	K_{b2} (kcal·mol^{-1}Å^{-2})	K_{b3} (kcal·mol^{-1}Å^{-3})	K_{b4} (kcal·mol^{-1}Å^{-4})
C-C2	1.5300	299.6700	-501.7700	679.8100
C-H	1.1010	345.0000	-691.8900	844.6000
C2-F	1.3900	403.0320	0.0000	0.0000
Si-O	1.6400	350.1232	-517.3424	673.7067
O-Ho	0.9494	540.3633	-1311.8663	2132.4446

Table S5 Angle parameters.

Angle	θ_0 (degree)	K_{a2} (kcal·mol^{-1}rad^{-2})	K_{a3} (kcal·mol^{-1}rad^{-3})	K_{a4} (kcal·mol^{-1}rad^{-4})
C2-C-C2	112.6700	39.5160	-7.4430	-9.5583
C2-C-H	110.7700	41.4530	-10.6040	5.1290
H-C1-H	107.6600	39.6410	-12.9210	-2.4318
C-C2-C	112.6700	39.5160	-7.4430	-9.5583
C-C2-F	109.2000	68.3715	0.0000	0.0000
F-C2-F	109.1026	71.9700	0.0000	0.0000
Si-O-Ho	122.8000	23.7764	-19.8152	9.6331

Table S6 Interatomic Lennard-Jones potential parameters

	Pair coeff	ε (kcal·mol^{-1})	σ (Å)	cutoff (Å)
Between Si and hydroxyl group	Si-O	0.1013	4.230	10
	Si-Ho	0.1066	3.825	10
Between Si and PVDF	Si-C	0.1013	4.230	10
	Si-C2	0.1013	4.230	10
	Si-F	0.1066	3.825	10
	Si-H	0.0616	3.200	10
Between hydroxyl group and PVDF	O-C	0.1138	3.680	10
	O-C2	0.1138	3.680	10
	O-F	0.1198	3.275	10
	O-H	0.0693	3.1725	10
	Ho-C	0.0265	2.554	10
	Ho-C2	0.0265	2.554	10
	Ho-F	0.0279	2.149	10
	Ho-H	0.0161	2.0465	10

ESI 3. Structures after relaxing
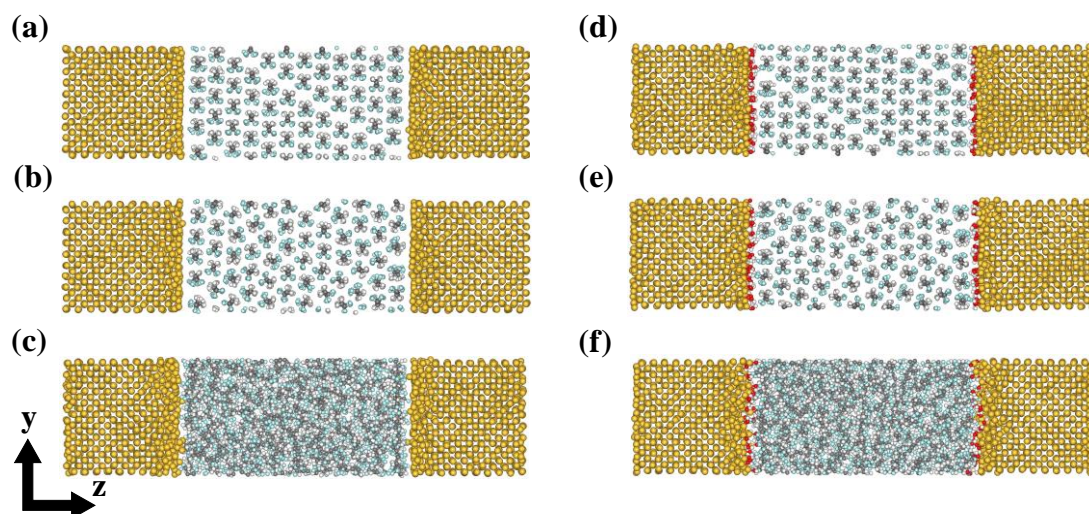
Fig. S1 Schematics of structure after relaxation at 300K of (a) intrinsic silicon/poled PVDF (In-Si/P-PVDF) interface, (b) intrinsic silicon/unpoled PVDF (In-Si/U-PVDF) interface, (c) intrinsic silicon/amorphous PVDF (In-Si/A-PVDF) interface, (d) modified silicon/poled PVDF (Mod-Si/P-PVDF) interface, (e) modified silicon/unpoled PVDF (Mod-Si/U-PVDF) interface and (f) modified silicon/amorphous PVDF (Mod-Si/A-PVDF) interface.

ESI 4. Temperature and heat flux
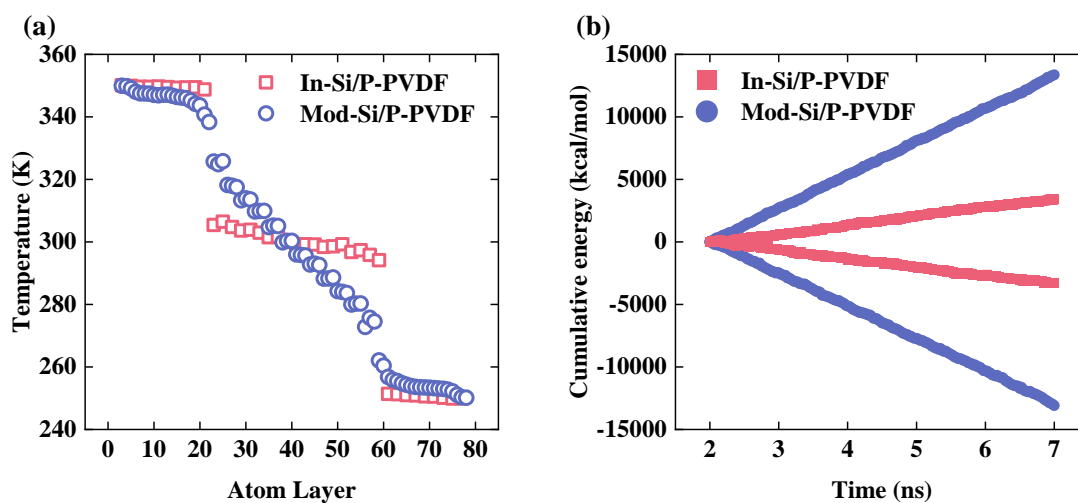
Fig. S2 (a) The temperature difference and (b) cumulative energy of the In-Si/P-PVDF and Mod-Si/P-PVDF structures along with z direction calculated by NEMD are recorded at 100K temperature difference.
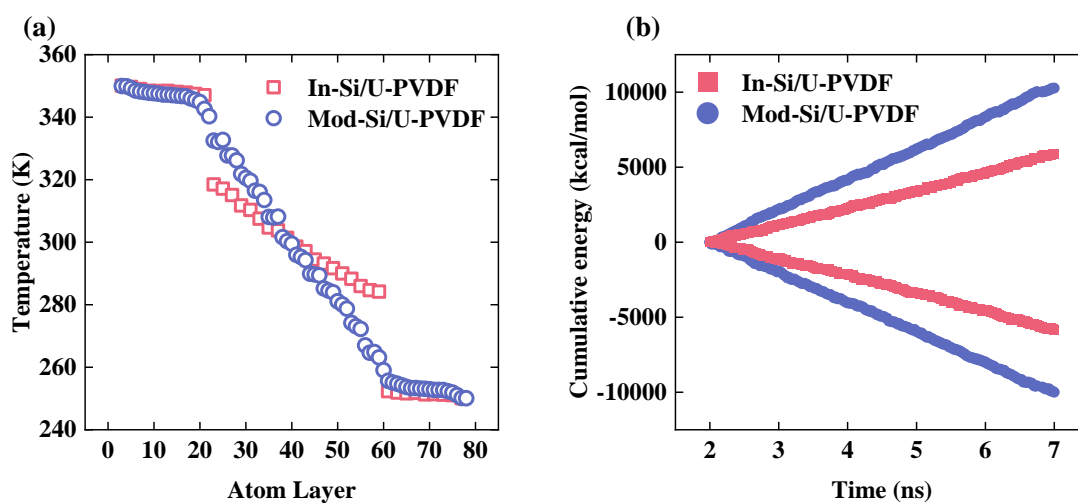

Fig. S3 (a) The temperature difference and (b) cumulative energy of the In-Si/U-PVDF and Mod-Si/U-PVDF structures along with z direction calculated by NEMD are recorded at 100K temperature difference.
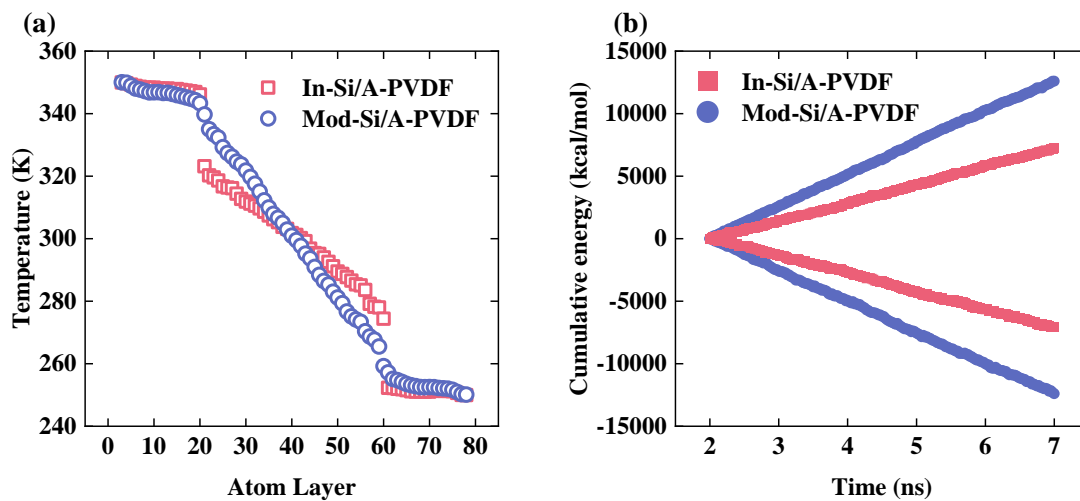
Fig. S4 (a) The temperature difference and (b) cumulative energy of the In-Si/A-PVDF and Mod-Si/A-PVDF structures along with z direction calculated by NEMD are recorded at 100K temperature difference.

ESI 5. Thermal conductivity of PVDF.
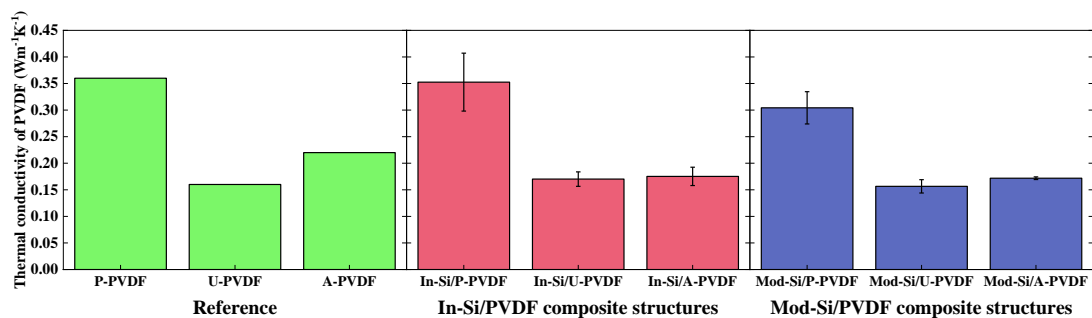
Fig. S5 Thermal conductivity of PVDF in all Si/PVDF composite structures. The thermal conductivity of U-PVDF and A-PVDF is comparable, while the thermal conductivity of P-PVDF exceeds both. The value of reference is from the previous study[4].

ESI 6. The interaction between Mod-Si and PVDF.

The interaction between the F atom and the OH group in Fig. 4 (b) and (c) is similar to that between the C atom and the OH group. Firstly, there is also a higher interaction between the OH group and the C atom in PVDF. As shown in Table S2, the high charge of the C atom (0.5e) in PVDF results in a stronger Coulombic force with the OH group.

Secondly, when averaging and calculating the value of force in MD simulation, all atoms are considered and counted. For instance, shown in Fig. R1, when averaging the interaction between an F atom, both the nearest neighbor F atom (F1) and the next nearest neighbor F atom (F2) to the interface are counted, the values are averaged of these two interactions. As a result, the force between the OH group and the F atom is not much higher than that between the OH group and the C atom.
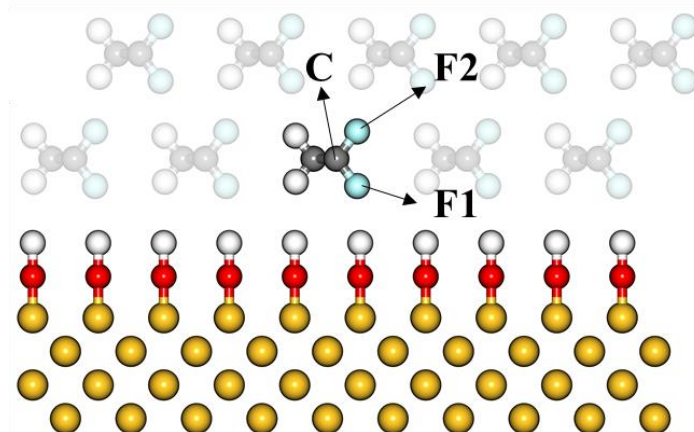

Fig. S6 Schematic of atomic force in Mod-Si/P-PVDF composite structures. Both the nearest neighbor F atom (F1) and the next nearest neighbor F atom (F2) to the interface are counted.

ESI 7. Phonon density of states in the full frequency range.

The vibrational density of states (VDOS) is calculated based on Parseval's theorem, the mass weighted power spectra $P(\omega)$ are calculated based on velocities. Then VDOS is expressed as

$$P(\omega) = \frac{1}{N}\sum_{i=1}^{N} m_i \left| \frac{1}{\sqrt{2\pi}} \int v_i(t)e^{-i\omega t} dt \right|^2$$

here ω is the angular frequency, N is the number of atoms, m is the atomic mass, v is the velocity, and t is the time interval. We recorded the trajectory of Mod-Si/P-PVDF structures, then performed fast a Fourier transform and multiple time average to obtain the power spectra. VDOS in the full-frequency range is given in Fig. S10.
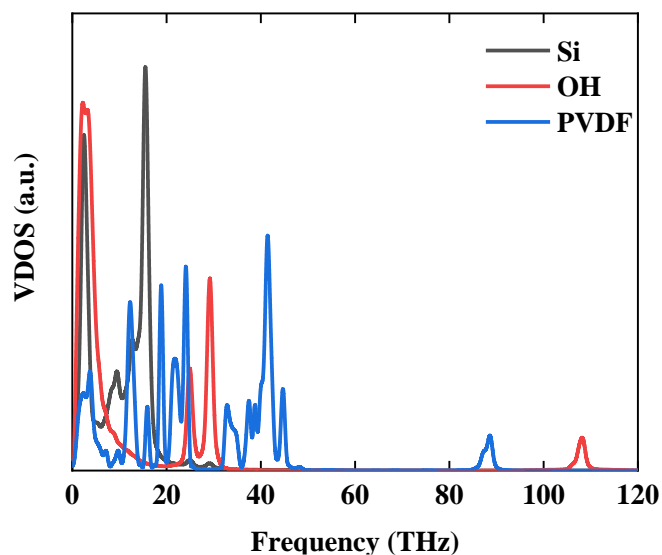

Fig. S7 VDOS comparison between atom groups of Si, OH, and PVDF in full frequency range.

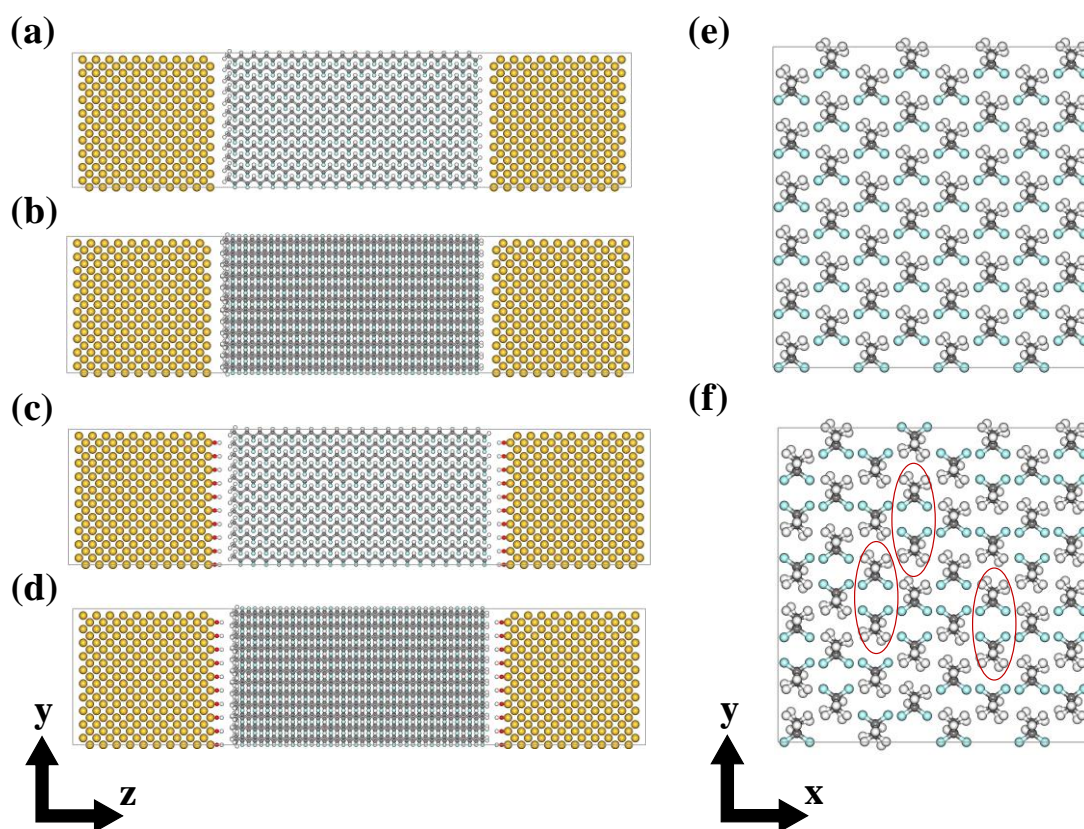## ESI 8. Interfacial thermal conductance of Si/Z-PVDF.

Fig. S8 Schematics of the interface structure are shown in the yz plane: (a) intrinsic silicon/poled PVDF chain oriented in the z-direction (In-Si/PZ-PVDF) interface, (b) intrinsic silicon/unpoled PVDF chain oriented in the z-direction (In-Si/UZ-PVDF) interface, (c) modified silicon/poled PVDF chain oriented in the z-direction (Mod-Si/PZ-PVDF) interface, (d) modified silicon/unpoled PVDF chain oriented in the z-direction (Mod-Si/UZ-PVDF) interface. Schematics of the PVDF structure are shown in the xy plane: (e) PZ-PVDF and (f) UZ-PVDF. The chain length of PVDF in the structure is 20 units.

In the case of finite-length PVDF, the terminal ends of PVDF segments are consistently designated as hydrogen atoms. Specifically, at one end, the carbon atom is bonded to three hydrogen atoms (CH3), while at the other end, it is bonded to two fluorine atoms and one hydrogen atom (CF2H).

Even for different end atoms of PVDF chains, the strategy to enhance interface thermal conductivity remains effective. As shown in the structures in Fig. S6, the left end of PVDF is CH3 and the right end is CF2H. As shown in Fig. S7 and Fig. S8, it is observed that a decrease in temperature gap at interfaces and an increase in heat flux, with hydroxylation of the silicon surface. Thus the interface thermal conductance is enhanced.
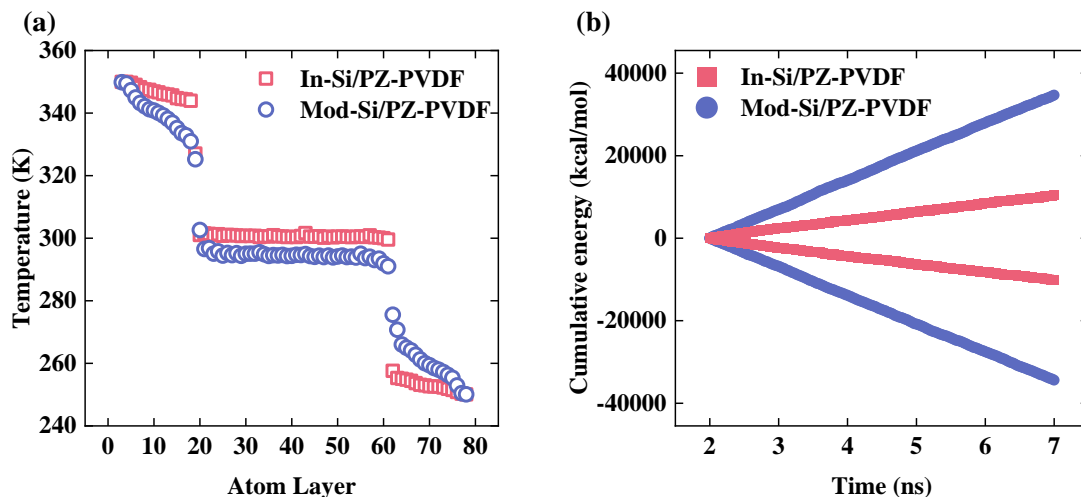

Fig. S9 (a) The temperature difference and (b) cumulative energy of the In-Si/PZ-PVDF and Mod-Si/PZ-PVDF structures along with z direction calculated by NEMD are recorded at 100K temperature difference.
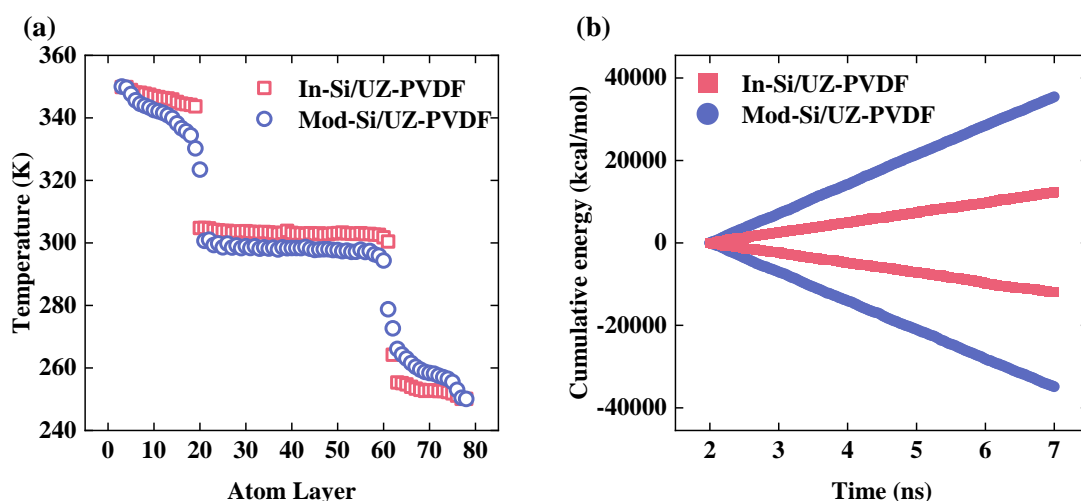

Fig. S10 (a) The temperature difference and (b) cumulative energy of the In-Si/UZ-PVDF and Mod-Si/UZ-PVDF structures along with z direction calculated by NEMD
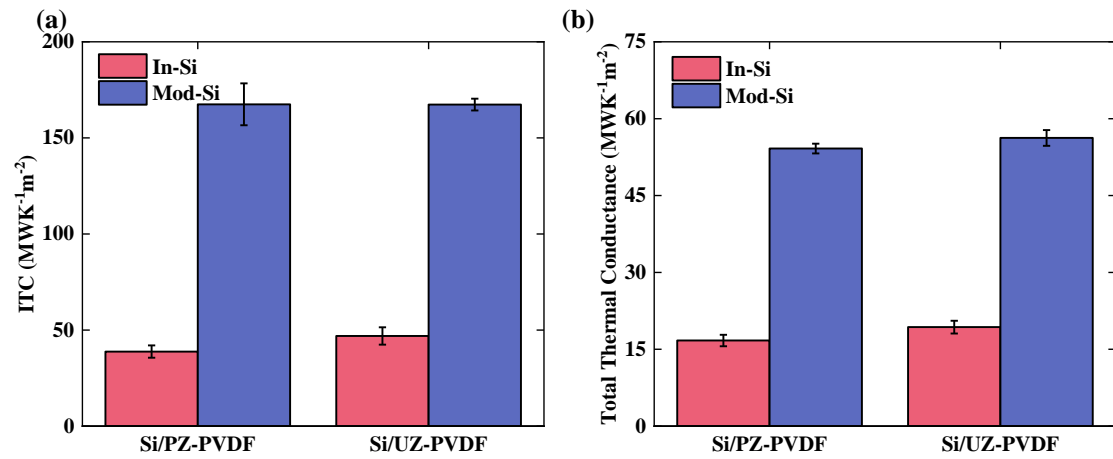
are recorded at 100K temperature difference.

Fig. S11 (a) ITC of Si/Z-PVDF interface: For Si/PZ-PVDF and Si/UZ-PVDF, through modification of Si surface ITC can be increased by 331% and 256%. (b) Total conductance of composite structures: For Si/PZ-PVDF and Si/UZ-PVDF composite structures, through modification of the Si surface total conductance of composite structures can be increased by 224% and 191%.

Reference

1. T. Luo and J. R. Lloyd, *Adv. Funct. Mater.*, 2012, **22**, 2495-2502.

2. A. P. Thompson, H. M. Aktulga, R. Berger, D. S. Bolintineanu, W. M. Brown, P. S. Crozier, P. J. in 't Veld, A. Kohlmeyer, S. G. Moore, T. D. Nguyen, R. Shan, M. J. Stevens, J. Tranchida, C. Trott and S. J. Plimpton, *Comput. Phys. Commun.*, 2022, **271**, 108171.

3. H. Sun, S. J. Mumby, J. R. Maple and A. T. Hagler, *J. Am. Chem. Soc.*, 1994, **116**, 2978-2987.

4. S. Deng, J. Yuan, Y. Lin, X. Yu, D. Ma, Y. Huang, R. Ji, G. Zhang and N. Yang, *Nano Energy*, 2021, **82**, 105749.